This is a repository copy of *Determining the mechanism and efficiency of industrial dye adsorption through facile structural control of organo-montmorillonite adsorbents*.

White Rose Research Online URL for this paper:
http://eprints.whiterose.ac.uk/119276/

Version: Accepted Version

Determining the mechanism and efficiency of industrial dye adsorption through facile structural control of organo-montmorillonite adsorbents

Peng Huang[1], Algy Kazlauciunas[1], Robert Menzel[2], Long Lin[1*]*

[1]Department of Color Science, School of Chemistry, University of Leeds, Leeds, LS2 9JT, UK

E-mail: l.lin@leeds.ac.uk

[2]School of Chemistry, University of Leeds, Leeds, LS2 9JT, UK

E-mail: R.Menzel@leeds.ac.uk

KEYWORDS: Inorganic/organic hybrid materials, dye effluent treatment, clay intercalation, adsorption mechanism, intra-particle diffusion

ABSTRACT: The structural evolution of cost-effective organo-clays (montmorillonite modified with different loadings of CTAB (cetyltrimethylammonium bromide)) is investigated and linked to the adsorption uptake and mechanism of an important industrial dye (hydrolyzed Remazol Black B). Key organo-clay characteristics, such as the intergallery spacing and the average number of well-stacked layers per clay stack are determined by low-angle X-ray diffraction (XRD), while differential thermo-gravimetric analysis (DTGA) is used to differentiate between surface-bound

and intercalated CTAB. Insights into the dye adsorption mechanism are gained through the study of the adsorption kinetics and through the characterization of the organo-clay structure and surface charge after dye adsorption. It is shown that efficient adsorption of anionic industrial dyes is driven by three key parameters: (i) sufficiently large intergallery spacing to enable accommodation of the relatively large dye molecules, (ii) crystalline disorder in the stacking direction of the clay platelets to facilitate dye access, (iii) and positive surface charge to promote interaction with the anionic dyes. Specifically, it is shown that at low modifier loadings (0.5 cation exchange capacity (0.5CEC)), CTAB molecules exclusively intercalate as a monolayer into the clay intergallery spaces, while with increasing modifier loadings, the CTAB molecules adopt a bilayer arrangement and adsorb onto the exterior clay surface. Bilayer intercalation results in sufficiently large expansion of the intergallery spaces and significant disordering along the (001) stacking direction to enable high and relatively fast dye uptake via intra-particle diffusion. Poor and slow dye uptake is observed for the organo-clays with monolayer structure, suggesting relatively inefficient dye adsorption at the clay edges. The optimized bilayer organo-clays (montmorillonite modified with 3CEC of CTAB) also show enhanced adsorption efficiencies for other important industrial dyes, highlighting the importance of structural control in organo-clays while also showing the adsorbents' great potential for use in industry where dye mixtures are encountered.

INTRODUCTION

Over 7×10^5 metric tons of synthetic dyes are produced worldwide every year for use in textile dyeing[1]. About 5%–10% of dye is released into the ecosystem along with dyeing wastewater, causing severe water pollution[2]. The discharge of dyeing wastewater to rivers and river basins poses significant risks both to local residents' health and the ecosystem. The damage to the

environment caused by dyehouse effluents is, in most cases, irreversible. Therefore, the effective treatment of dye-containing wastewater has become a major priority for governments[3]. The principal pollutants generated during production operations in the textile industry are colorants, recalcitrant organics, toxic and inhibitory compounds, soaps, surfactants, chlorinated compounds, detergents, and salts. This specific type of pollution is characterized by high chemical oxygen demand, biochemical oxygen demand, unpleasant smell, suspended solids (mainly fibers), toxicity, and especially colour[4]. Reactive azo dyes (such as Remazol Black B) make up approximately 30% of the total dye market[5]. As much as 50% of the dye can be lost in the current commercial dyeing processes.

Dyeing wastewaters are difficult to clean because of the relatively inert nature of the chromophores[6]. Some dyes are recalcitrant molecules (particularly azo dyes) and are generally designed to withstand chemical, microbial, and photolytic degradation[7]. The more frequently employed chemical classes of dyes on an industrial scale are azo dyes, sulfur dyes, anthraquinone dyes, triphenylmethyl (trityl) dyes, indigoid dyes, and phthalocyanine derivatives. However, the type of dyes in the effluent could vary daily, or even hourly, depending on production routines and fashion cycles[8]. In general, a suitable technique for the treatment of dyeing wastewater should meet several conditions: (1) be readily available, (2) be economically feasible to use, (3) be effective for removal of various target dyes, (4) possess high selectivity at different concentrations, and (5) give high dye removal efficiency in terms of uptake capacity and kinetics. So far, ranges of well-established conventional dyeing wastewater treatment technologies have been developed. These include physical[9-10], chemical[11] and biological processes[12], as well as some new techniques such as sonochemical[13] or advanced oxidation processes[14]. The major criteria for the selection of

a suitable technique will depend on operating costs and the time required for the desired extent of treatment[15].

Montmorillonites (MMTs), a very soft phyllosilicate group of minerals that typically form in microscopic crystals, exhibit strong adsorption capability due to the large surface area and the considerable surface energy[16]. However, natural MMT possesses negative charges on the surface and exhibits low adsorption capacity for dyeing wastewater. The occupation of exchange sites on the MMT surface by organic cations changes the MMT's surface properties from being negative to becoming positive. Therefore, there has been much interest in the use of modified MMTs as adsorbents to remediate negatively charged organic contamination. Previous studies have shown that the removal of acid dyes can be promoted by the use of sulfuric acid-activated MMT compared with untreated MMT[17]. Wang and Wang[18] prepared MMTs modified by a series of alkyl ammonium bromides with different alkyl chain lengths for the adsorption of Congo Red anionic dye in aqueous solutions. Other authors have successfully modified MMT using more unconventional modifiers[19], such as gemini surfactants, for the adsorption of organic contaminants[20-21]. The results showed that the adsorption capacity of surfactant-modified MMTs for organic contaminants was greatly improved compared with that of pristine MMT.

Although organo-clays have been used for the adsorption of anionic dyes[22], it is important to gain further insights into how their dye adsorption performance is linked to changes in their structural properties. The quantitative relationship between the cationic modifier in the organo-clay and the dye has rarely been reported. To effectively identify more appropriate surfactants for the modification of clays, to optimize the loading of the more expensive cationic organic modifier on the relatively cheap clays, and to improve the adsorption efficiency of the clays via tailoring the structure, it is vital to bridge the gap between structure of the organo-clays and their dye

adsorption properties. It is recognized that the surface properties and the basal spacing of organo-clays are important parameters for the adsorption capacity[23]. However, the influence of the stacking state of the clay platelets on the adsorption performance has not been discussed, but will be taken into account in this investigation. In this study, surfactant modified clays have been prepared, using CTAB, to provide a more efficient route and low-cost adsorbent for the treatment of dyehouse wastewaters. MMT and CTAB are both cheap, readily available commercial products which are widely used in industry. Thus, the functionalization of montmorillonite, using CTAB, would be economically feasible. The main dye investigated in this study was Remazol Black B, the most widely used reactive azo dye; importantly the dye was hydrolyzed before the adsorption measurements to simulate real dyehouse effluents. Experimental insights into the structure and properties of the organo-clays were obtained through a combination of material characterization techniques. The structural change in the organo-clays (e.g. location and arrangement of modifier molecules, disordering in the stacking direction of the clay platelets) was investigated as function of CTAB loading and correlated with their liquid-phase adsorption uptake capacities and kinetics for hydrolyzed Remazol Black B (and other anionic industrial dyes) in aqueous solution.

EXPERIMENTAL SECTION

Materials

Sodium-montmorillonite (Na-MMT), a natural clay with an average particle size of 7 μm, was obtained from Alfa Aesar (UK). Triethylenetetramine ($\geq$ 97.0%) and sodium hydroxide were purchased from Sigma-Aldrich (UK). Copper(II) sulfate (98%, anhydrous) and cetyltrimethylammonium bromide ($C_{19}H_{42}BrN$, CTAB) were supplied by Fisher Scientific (UK).

Commercially available Remazol Black B, an anionic dye having a molecular formula $C_{26}H_{21}N_5Na_4O_{19}S_6$ and a purity of 88%, was obtained from Regency FCB Ltd (UK).

Preparation of organo-montmorillonite

The loading fractions of CTAB during organo-montmorillonite (OMMT) preparation were chosen relative to the cation exchange capacity (CEC) of unmodified Na-MMT (85.3 mmol/100g, for experimental details see ESI). The organo-montmorillonite (OMMT) samples were prepared using the following procedure[24]: Na-MMT (1 g) was placed in a round-bottomed flask, into which a solution of ethanol/water (100 mL, v/v = 1:1) was added. The mixture was stirred vigorously at 60 °C in a thermostated oil bath for 1 hour, to form a uniform suspension. This was followed by addition of different amounts of CTAB, equivalent to 0.5 CEC, 1.0 CEC, 2.0 CEC, 3.0 CEC, and 4.0 CEC of Na-MMT, respectively. The mixture was stirred for a further 6 hours and then centrifuged at 4000 rpm for 15 minutes. Each of the OMMT samples obtained were washed five times, with 200 mL of hot water each time, to remove any excess/residue CTAB. The washed samples were dried in an oven at 105 °C to a constant weight, before being ground in an agate mortar for subsequent use. The resultant samples were denoted as 0.5OMMT, 1.0OMMT, 2.0OMMT, 3.0OMMT, and 4.0OMMT, respectively.

Adsorption of hydrolyzed Remazol Black B dye from aqueous solutions, using Na-MMT and using OMMT

To simulate real dyehouse effluent, aqueous hydrolyzed dye solutions were obtained via the following procedure[25]. 0.1 g of the Remazol Black B reactive dye (based on the purity) was dissolved in 50 mL of distilled water and the pH of the solution adjusted to 12 using 1 mol/L sodium hydroxide solution. The solution was then stirred under reflux, at 80 °C, for 1 hour, and

left to cool to ambient temperature. The cooled solution was neutralized using 1 mol/L hydrochloric acid. The desired hydrolyzed dye sample was obtained by diluting the concentrated stock solutions. In each of the adsorption experiments, Na-MMT or OMMT was dispersed in a small amount of water (40 mg of the clay in 3.96 g of water), then added into 100 mL of the aqueous solution of hydrolyzed dye (dye concentration 100 mg/L). The samples were stirred at 20 °C and pH 7, for 1 hour or 26 hours. After the adsorption process, 1 mL of the mixture was extracted and diluted to 10 mL. The sample was filtered, and its absorbance value measured at the λ_{max}, 597 nm, using a UV-Vis spectrophotometer. The concentration of the remaining hydrolyzed dye in the aqueous solution was calculated using a linear regression equation based on a calibration plot (see ESI). For the study of the adsorption kinetics, aliquots of the mixture were taken from the dye solution at regular time intervals, and diluted to 10 mL with distilled water. Each sample was filtered and the absorbance value determined. Plotting the quantity of adsorbed dye against the square root of the adsorption time, the adsorption kinetics can be analyzed according to the intra-particle diffusion model[26]:

$$q_t = k_i t^{1/2} + C \qquad (1)$$

Here, t is the time that has elapsed; q_t is the amount of the hydrolyzed dye adsorbed onto the organo-clay; k_i is the rate constant and C is the intercept of the regression curve. The intra-particle diffusion model assumes that three steps are involved in the adsorption process onto porous adsorbent particles: (1) diffusion of the adsorbates from the bulk solution to the external surface of the adsorbent; (2) diffusion of the adsorbate molecules from the external surface of the adsorbent to the interior pores; (3) the adsorption of the solute species into the interior surface of the pores via the active sites.

Materials characterization

Samples were analyzed using a PerkinElmer Spectrum One FT-IR Spectrometer. The unit was operated in a reflectance mode, with the scanning range between 550 cm^{-1} and 4000 cm^{-1}. Thermo-gravimetric analyses (TGA) of the samples were performed using a TGA Q50 model (TA instruments, USA), under a nitrogen atmosphere. The balance purge flow rate was 40 mL/min, and the sample purge flow rate was 60 mL/min. Each of the powder samples (approximately 10 mg) was heated from 25 °C to 800 °C, at a heating rate of 10 °C/min. Thermograms were differentiated to obtain differential TGA (DTGA) curves allowing to identify the different stages of thermal conversions more clearly. Differential scanning calorimetric (DSC) analyses of the samples were conducted using a DSC Q20 model (TA instruments, USA), under a nitrogen atmosphere. The heating rate was 10 °C/min, increasing from 25 °C to 400 °C, with a nitrogen flow rate of 50 mL/min. The low-angle X-ray diffraction (XRD) patterns of Na-MMT, of the OMMT, and of the dyed OMMT samples were measured, over the scanning range of $2\theta = 1.5°$ - 15°, using a Bruker D8 Advance X-ray diffraction equipment, at ambient temperature. The tests were performed using Cu Kα radiation ($\lambda = 0.154$ nm), at a generator voltage of 40 kV and a current of 40 mA. The step size was 0.026°. The d-spacing of the clay layers was calculated according to Bragg's law. Crystallite domain size, corresponding to the (001) reflections, was calculated from the broadening of (001) XRD peak using the Scherrer equation:

$$D_{001} = k\lambda/\beta\cos\theta. \qquad (2)$$

Here, D_{001} is the mean crystallite domain size along the (001) direction; k is a dimensionless shape factor (k = 0.89); λ is the wavelength ($\lambda = 0.154$ nm); β is the line broading at full-width at half-maximum (FWHM), in radians; and θ is the diffraction angle. From the crystallite domain size and the d-spacing of the clay layers, the number of clay platelets per average stack (n), i.e. the average

number of clay platelets stacked with high crystalline order, was calculated according to the equation[27]:

$$n = 1 + D_{001}/d_{001}. \tag{3}$$

The zeta potential values of Na-MMT and of OMMT, dispersed in distilled water or in aqueous solutions of the hydrolyzed Remazol Black B dye (4 mg of the clay in 10 mL of water or the aqueous dye solution), were obtained using a Malvern Zetasizer-Nano ZS model (Malvern Instruments Ltd, UK).

RESULTS AND DISCUSSION

Structural characterization of organo-clays

The average cation exchange capacity (CEC) of the unmodified Na-MMT clay used in this study was determined to be 85.3 mmol/100g. To produce a series of organo-clay samples with distinct structure differences, Na-MMT clay was modified with CTAB at loadings relative to this value. Specifically, CTAB loadings of 0.5, 1, 2, 3 and 4 equivalents of the Na-MMT CEC value were used to produce organo-clay (OMMT) samples referred to as 0.5OMMT, 1.0OMMT, 2.0OMMT, 3.0OMMT and 4.0OMMT, respectively.

IR spectra of Na-MMT and of OMMT (Figure 1a) clearly confirmed successful modification. For the sample of Na-MMT, characteristic absorption bands appeared at 3623 cm^{-1} (–OH stretching of Al,Mg(OH))[28], 1632 cm^{-1} (–OH bending)[29], 997 cm^{-1} (stretching vibration of Si-O-Si) and 518 cm^{-1} (bending vibration band of Si-O). All OMMT samples showed additional absorption bands at 2929 cm^{-1} and 2856 cm^{-1} (asymmetric and symmetric stretching vibration of –CH$_3$ and –CH$_2$-), and at 1474 cm^{-1} (bending vibration of C-H of the methyl group of the ammonium groups), evidencing the incorporation of CTAB into the structure of the clay.
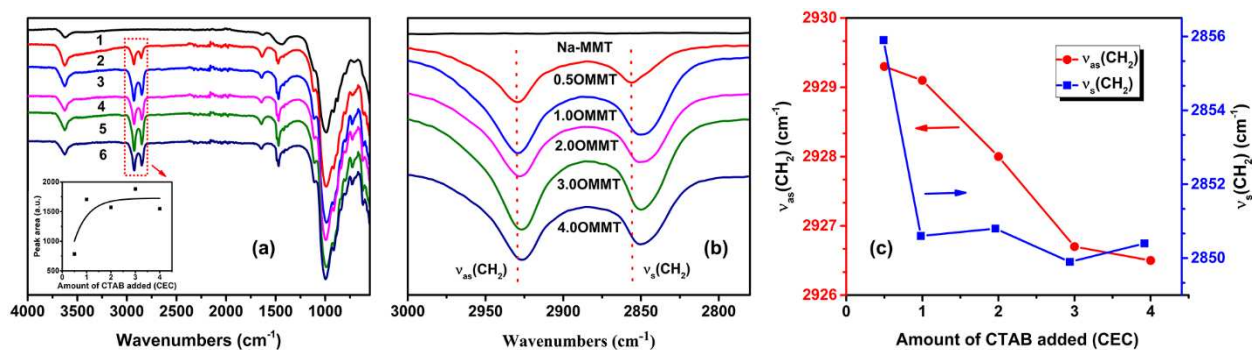
Figure 1. (a) IR spectra of Na-MMT and of OMMT: (1-Na-MMT; 2-0.5OMMT; 3-1.0OMMT; 4-2.0OMMT; 5-3.0OMMT; 6-4.0OMMT), (b) IR spectra of OMMT, in the region of 3000 cm^{-1} – 2800 cm^{-1}, (c) the change of v_{as}(-CH$_2$-) and v_s(-CH$_2$-) as a function of CTAB loading.

On increasing the CTAB loading, the peak intensity and peak area of the OMMT-related absorption bands at 2929 cm^{-1} and 2856 cm^{-1} became stronger and sharper (Figure 1a), indicating an initial sharp increase in CTAB incorporation followed by a levelling off at greater CTAB loadings (Figure 1a, inset). The frequency and band width of the –CH$_2$- stretching vibration band are related to the trans/gauche conformer ratio of the alkyl chains[30-31]. On increasing the amount of CTAB loading, these bands shift towards lower frequencies (Figure 1b and Figure 1c), suggesting a transition from a disordered liquid-like conformation of CTAB alkyl chains at low loadings to more ordered state at high loadings where the modifier alkyl chains exhibit well-aligned trans conformations[30-31].

In order to quantify the modifier loading and investigate the structural properties of the organo-clays, TGA experiments were conducted under inert atmosphere (Figure 2a). Unmodified Na-MMT exhibited a mass loss of 1.7% in the temperature range of 25°C-130°C, due to the loss of interlayer water, followed by a second mass loss of 7.6% between 130°C - 700°C, attributed to the dehydration of the MMT layers, including condensation of both the intralamellar Al(OH) and structural Al(OH) in the clay[32]. For the OMMT samples, TGA (Figure 2a) and differential TGA

(DTGA, Figure 2b) clearly showed additional weight losses between 200°C-460°C, not present in Na-MMT, confirming again the presence of the bound organic modifier within the clay structure. The amount of organic modifier successfully incorporated into the organo-clays after synthesis and washing was calculated by integration under the DTGA curves in this temperature region (Figure 2c). The results (Figure 2c) show an initial steep increase in incorporated modifier that levels off at higher amounts of added CTAB, consistent with the IR results (Figure 1a, inset). These findings indicate that incorporation of the organic modifier is highly effective when relatively small amounts of CTAB are present during organo-clay synthesis, i.e. almost all CTAB present in the synthetic mixture is incorporated into the clay structure. However, modifier incorporation becomes increasingly less efficient when the amount of organic modifier in the synthesis is increased, levelling off at a CTAB loading of 3.0CEC, beyond which point no more CTAB can be incorporated into the clay structure. The maximum amount of organic modifier that can be incorporated into the clay was found to be 22 wt% (equivalent to 113mmol CTAB/100g clay).

Interestingly, TGA and DTGA for most organo-clay samples (Figure 2a, 2b) showed two distinct steps in the combustion region (200°C-460°C): a first weight loss between 200°C-320°C is followed by a second, distinct weight loss between 320°C-460°C. The first weight loss occurs at about 40°C higher temperature compared to the combustion of free, unbound CTAB (see ESI), and was assigned to modifier molecules attached to the clay surface. The second mass loss occurs at nearly 150°C above the combustion temperature of free CTAB, suggesting considerable protection of the related organic species, indicative of organic cations intercalated between the clay layers.
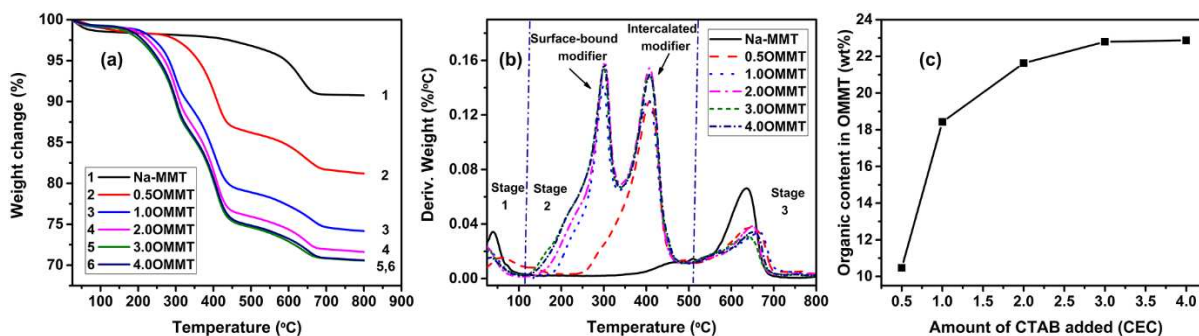
Figure 2. (a) TGA thermograms of Na-MMT and of OMMT, (b) DTGA traces of Na-MMT and of OMMT, (c) The mass ratio percentage of organic modifier incorporated in OMMT at different original CTAB loadings.

The latter assignment is consistent with general observations that organic molecules located in the confined interlayer spaces of the clay possess greater thermal stability than free organic molecules[33]. TGA and DTGA data of 1.0OMMT, 2.0OMMT, 3.0OMMT and 4.0OMMT all showed a similar degradation profile (Figure 2a, 2b), indicating the presence of both surface-bound and intercalated organic modifiers. However, 0.5OMMT only showed one combustion event at around 410°C, indicating that, at low modifier loadings, only intercalation into the clay interlayers occurs.
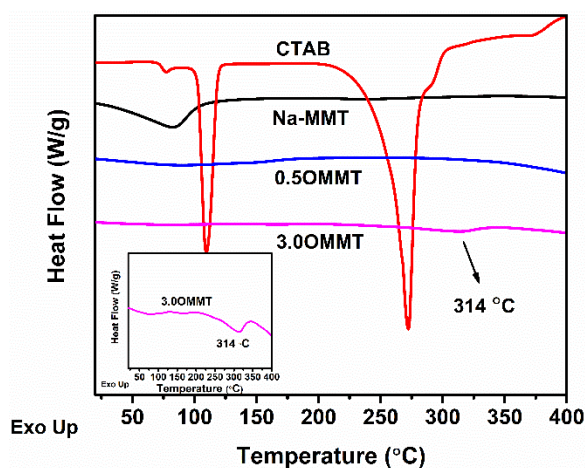

Figure 3. DSC thermograms of CTAB, of Na-MMT and of OMMT. Inset: enlarged DSC thermogram of 3.0OMMT.

This observation was confirmed via differential scanning calorimetric (DSC) measurements (Figure 3). The DSC thermogram of free CTAB exhibits three characteristic, endothermic troughs with the most prominent one at 272°C, related to the melting and decomposition of the CTAB molecules. For the 0.5MMT, no melting trough was observed. However, the DCS thermogram of 3.0OMMT showed a small endothermic trough at 314°C, i.e. around 40°C above the melting trough of free CTAB. This observation is consistent with the TGA findings, suggesting that the trough at 314°C corresponds to the melting and decomposition of the CTAB molecules attached on the clay surface.

Intercalation behavior of CTAB into the organo-clays

The interlayer spacing, d_{001}, of the parent clay Na-MMT and of OMMT were determined using low-angle XRD. For Na-MMT (Figure 4a), a broad peak was observed at $2\theta = 7.58°$, corresponding to an interlayer spacing (d-spacing) of 1.17 nm. Upon the addition of CTAB, the peak positions shifted to lower angles depending on the CTAB loading, implying that the basal spacings of the clays were expanded due to intercalation. With a CTAB loading of 0.5 CEC, the strong and sharp peak at $2\theta = 6.01°$ corresponds to $d_{001} = 1.47$ nm. When the CTAB loading was increased to 1.0 CEC, the interlayer spacing of the organo-clay further expanded to 1.87 nm. However, the position of the peaks almost remained constant with greater CTAB loadings, suggesting that there was a saturation limit for the intercalation of the CTAB molecules inside the clay, consistent with the FTIR and TGA results discussed above.
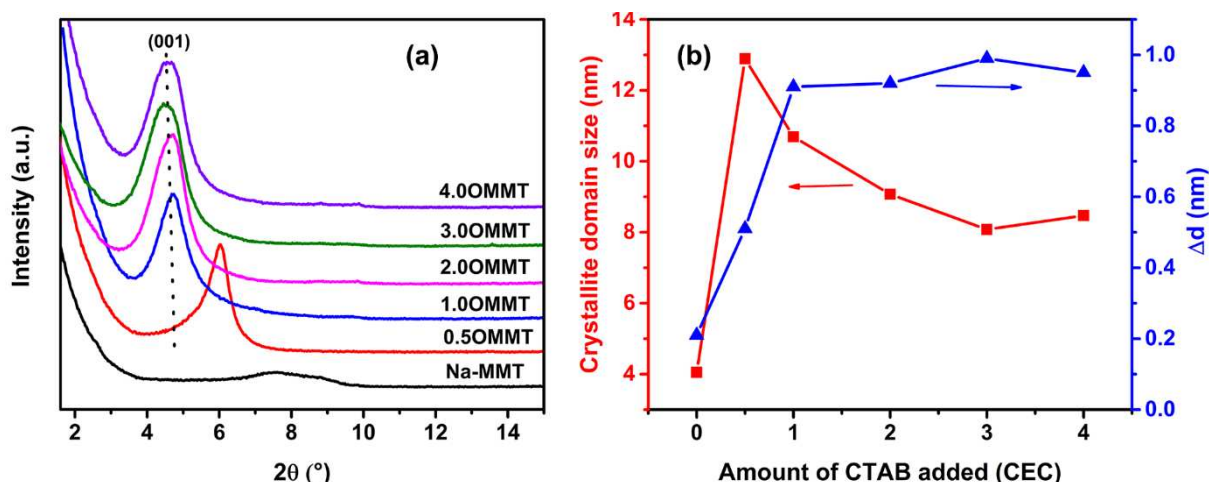
Figure 4. (a) Low-angle XRD patterns of Na-MMT and of OMMT, (b) Crystallite domain size and Δd of Na-MMT and of OMMT.

The intercalation of CTAB into the interlamellar space of the clay is likely to be mainly through a cation exchange process, in which the Na^+ ions were replaced by the positively charged CTAB molecules, to compensate for the excess negative layer charges. The thickness of a single, unmodified montmorillonite structural unit is about 0.96 nm[28], and the accommodation of water or low valence cations in the interior of the crystals swells and expands the clay slightly[34]. The width of the interlamellar space, Δd, occupied by the CTAB molecules can be obtained by subtracting the thickness of the single montmorillonite unit (0.96 nm) from the d_{001} spacing of the organo-clay. The Δd values increased to 0.51 nm when 0.5 CEC of CTAB was used in the synthesis and reached up to 0.91 nm for the 1.0OMMT sample, but remained almost constant with greater CTAB loadings (Figure 4b).

The chain of the CTAB molecule has a ''nail-shaped'' character, with the quaternary ammonium group as the ''head'' and the alkyl chain as the ''body''. The conformation of the CTAB molecule is influenced by the thermodynamic parameters in the system, and the dimensions of the molecular chain vary accordingly. The length of the fully stretched CTAB chain is about 2.53 nm, the height

14

of the ''head'' and the ''body'' changes with the orientation of the alkyl chain. When the zigzag arrangement of the alkyl chain is perpendicular to the basal plane of clay platelet, the height of the ''head'' is 0.51 nm and the height of the ''tail'' is 0.46 nm [35]. These former values agree very well with the interlamellar width of 0.5OMMT ($\Delta d = 0.51$ nm), suggesting the intercalation of a CTAB monolayer (with the CTAB alkyl chain adopting a zigzag orientation perpendicular to the plane of the clay platelet). The interlamellar width of the 1.0OMMT ($\Delta d = 0.91$ nm) correlates very well with the sum of the height of one CTAB head group and the height of one CTAB alkyl ''tail'' chain (0.97 nm). It is therefore likely that the intercalated CTAB molecules adopt a bilayer arrangement, with the ''head'' and ''tail'' of two CTAB molecules in opposite directions, due to steric hindrance and electrostatic repulsion (Figure 5). The interlayer distances (Table 1) indicate that similar CTAB bilayer intercalation arrangements are found in all organo-clays with larger modifier loadings.
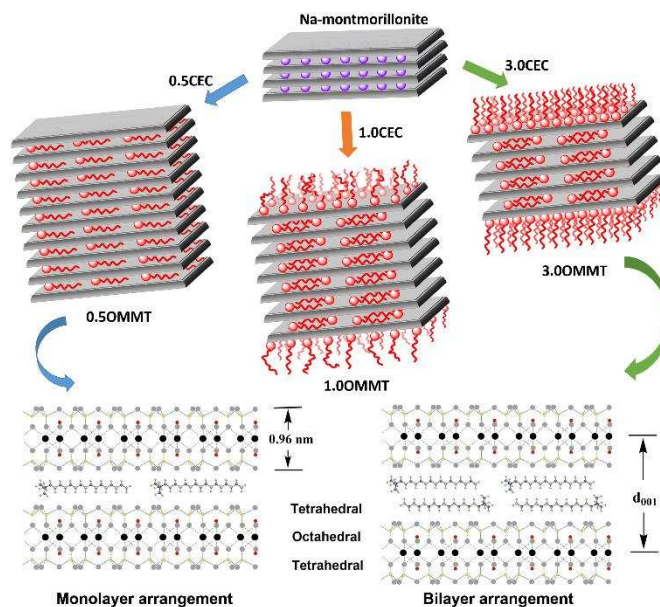

Figure 5. Representation of the formation of different OMMTs.

The crystallite domain size along the (001) direction of the clay crystallites were calculated from the broadening of the (001) XRD peak using the Scherrer equation (Figure 4b). The crystallite

domain size increased dramatically at a CTAB loading of 0.5 CEC, but then reduces gradually for larger CTAB loadings. This observation implies that different modifier loadings significantly impact on the crystallinity of the organo-clays in the (001) direction, i.e. in the stacking direction of the clays. In order to assess these changes in crystallinity accurately, the changes in interlamellar spacing, as discussed above, also need to be taken into account. When dividing the (001) crystallite domain size, D_{001} (i.e. the crystallite size in the direction of the platelet stacking) by the basal plane spacing of the platelets, d_{001}, the number of clay platelets in the crystalline domain (parameter n in Table 1), i.e. the average number of platelets stacked with high crystalline order, can be estimated, providing a clear and unambiguous indication for the stacking disorder of the clay platelets. In the case of the organo-clays, the average number of well-stacked platelets increased significantly at low CTAB loading (0.5CEC) but decreases at larger loadings (Table 1), reflecting the significant structural changes in the organo-clays (Figure 5). A potential explanation for this trend is that at low modifier loadings the monolayer arrangement leads to a bridging interaction of the organic cations between different clay basal planes, resulting in an interconnecting function and an increase in stacking order. However, the bilayer arrangement at larger modifier loadings and the corresponding larger interlamellar distances are likely to introduce disorder in the stacking direction of the layers, resulting in a lower average number of stacked platelets.

Table 1. Low-angle XRD parameters of Na-MMT and of OMMT.

	Na-MMT	0.5OMMT	1.0OMMT	2.0OMMT	3.0OMMT	4.0OMMT
2θ (°)	7.58	6.01	4.72	4.70	4.52	4.61
β (rad)	0.038	0.012	0.014	0.017	0.019	0.018
d_{001} (nm)	1.17	1.47	1.87	1.88	1.95	1.91
Δd (nm)	0.21	0.51	0.91	0.92	0.99	0.95
D_{001} (nm)	4.05	12.89	10.69	9.07	8.08	8.47
n	4	10	7	6	5	5

Note: β is the line broading at full-width at half-maximum (FWHM), in radians; Δd–width of the interlamellar space, $\Delta d = d_{001} - 0.96$ nm; D_{001} is the mean crystallite domain size along the (001) direction, nm; n is the number of clay platelets per average stack, $n = 1 + D_{001}/d_{001}$.

Dye adsorption characteristics of organo-clays

To correlate the structural changes of the organo-clays with their dye adsorption performance, batch dye adsorption experiments were carried out for 1 hour (a relatively short, but commercially-relevant time scale) and 26 hours (time to reach equilibrium as indicated by initial kinetic experiments); the uptake of hydrolyzed Remazol Black B dye from aqueous solution onto the clay samples was followed by UV-Vis spectrophotometry (Figure 6a). As expected, the Na-MMT control sample did not exhibit any dye adsorption capacity, while significant dye removal was observed after incorporation of CTAB into the structure. Zeta-potential measurements (ESI) show that the surface charge of all organo-clay samples is reduced upon dye adsorption, highlighting the importance of electrostatic interactions as important driving forces for anionic dye adsorption for all organo-clay loading fractions (charge neutralization mechanism)[36]. In addition, the hydrophobic alkyl chain of the organic modifier in the organo-clay is also likely to interact with the hydrophobic parts of the hydrolyzed dye facilitating dye uptake further (partition mechanism)[23]. The increase in dye uptake upon increased CTAB loading (Figure 6a) followed the

same trends as the structural characterization results (e.g. Figure 1a, Figure 2), clearly confirming the correlation of organo-clay structure and adsorption performance. The largest equilibrium dye uptake capacity was found for 3.0OMMT (77±2 mg/g). This dye uptake capacity is 100% larger than reported in previous studies on the removal of hydrolyzed Remazol Black B using other adsorbents such as activated sludge[37]. Consistent with the structural characterization of the organo-clays, further increases in the nominal CTAB loading to 4.0 CEC did not show any additional dye removal. Interestingly, the dye uptake capacity of the organo-clays exhibits a clear correlation with the number of clay platelets per average stack (Figure 6b), indicating that disorder in the stacking direction of the clay platelets plays an important role for efficient dye uptake, most likely due to improved access to the adsorption sites in disordered clay stacks. Further, the correlation suggests that dye uptake capacity of the organo-clay may be further improved if full clay exfoliation (n = 1) is achieved.
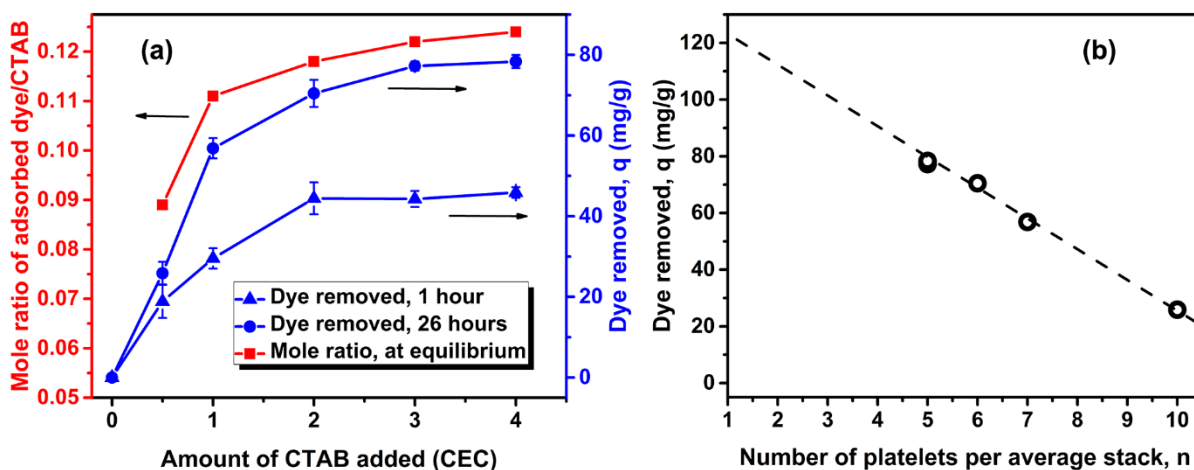

Figure 6. (a) Hydrolyzed Remazol Black B dye removed from aqueous solutions, using Na-MMT and using OMMT. The samples were stirred for either 1 hour or 26 hours, at 20 °C, at pH 7. The initial hydrolyzed dye loading was 100 mg/L. The amount of adsorbent was 40 mg/100 mL; Quantitative relationships between the amount of hydrolyzed Remazol Black B dye adsorbed on

OMMT and the amount of organic modifier incorporated in the OMMT, (b) Relationship between the number of platelets per average organo-clay stack and the amount of hydrolyzed Remazol Black B dye removed from aqueous solutions at equilibrium, using OMMT.

The number of dye molecules adsorbed per modifier molecule present in the organo-clay is shown in Figure 6a (red curve), providing a rough estimate how well the modifier molecules are utilized for dye adsorption. When the CTAB loading was increased from 0.5 CEC to 3.0 CEC the adsorption efficiency per mole of CTAB increased by 37%; i.e. that the utilization of the CTAB molecules for dye adsorption was significantly increased on average at greater modifier loadings. This increased efficiency directly correlates with the observed structural changes. The increased expansion of the clay interlamellar width, the availability of CTAB on the clay surface and the disordering along the stacking direction of the platelets at greater modifier loadings provided improved accessibility of the anionic dye to the CTAB molecules.

This hypothesis was further confirmed by the dye adsorption kinetics (Figure 7 and ESI) obtained for 0.5OMMT and 3.0OMMT, which were selected as limiting cases of organo-clays with intercalated monolayer and organo-clays with intercalated bilayer and surface-bound organic modifier, respectively. The collected kinetic data fitted best to a pseudo-second-order kinetic model (ESI), suggesting that chemisorption is the rate controlling parameter. Analysis of the kinetic data according to the intra-particle diffusion model (Figure 7) further confirms the structural changes discussed. For the 3.0OMMT sample, the experimental data best fit a multi-linear regression (Figure 7b). This implies that three steps were involved in the adsorption process[38]. The first linear fit with the steeper gradient indicates the fast diffusion of the dye molecules from the bulk solution onto the external surface of the 3.0OMMT, in line with the easier accessibility of CTAB molecules on the exterior surface in this sample. The second, lower-gradient

linear fit represents the slower transport of the dye molecules into the internal particle pores, i.e. into the interlamellar spaces of the 3.0OMMT clays. The third linear fit shows the final equilibrium stage, where the dye molecules adsorb onto the active sites in the interlamellar spaces. In contrast, only one, comparatively slow step was observed for the adsorption of the hydrolyzed dye onto the 0.5OMMT (Figure 7a), further demonstrating the significant structural differences between organo-clays with different modifier loadings (Figure 5). These fundamental differences were further confirmed by investigating the structural changes of the different organo-clay samples after dye adsorption (without washing), as measured by low-angle XRD (Figure 7c). The different XRD patterns of the dyed 0.5OMMT and 3.0OMMT samples reflect the difference in lamellar widths of the two organo-clays in relation to the molecular size of the dye. The dimension of the hydrolyzed Remazol Black B molecule (maximum dimension 0.82 nm, see ESI) is greater than the interlamellar space of 0.5OMMT (Δd=0.51nm) but smaller than that of 3.0OMMT (Δd=0.98nm). Consequently, the dye molecule is physically inhibited from penetrating into the interlamellar space of 0.5OMMT and is likely to mainly adsorb at the edges of the organo-clay platelets, resulting in no significant change to the XRD patterns after dyeing (Figure 7c). In contrast, the decrease in XRD peak intensity with time for the dyed 3.0OMMT sample (Figure 7c) suggests initial surface adsorption of the dye without significant impact on crystallinity (a clear XRD peak remains after 1h) followed by the slower adsorption of dye into the interlamellar spaces. The introduction of the dye into the interlamellar spaces after 26 h induces significant additional disorder in the stacking direction of the clay platelets, as indicated by the significant broadening and decreased intensity of the related XRD peak. These findings correlate well with the kinetic observations discussed above.
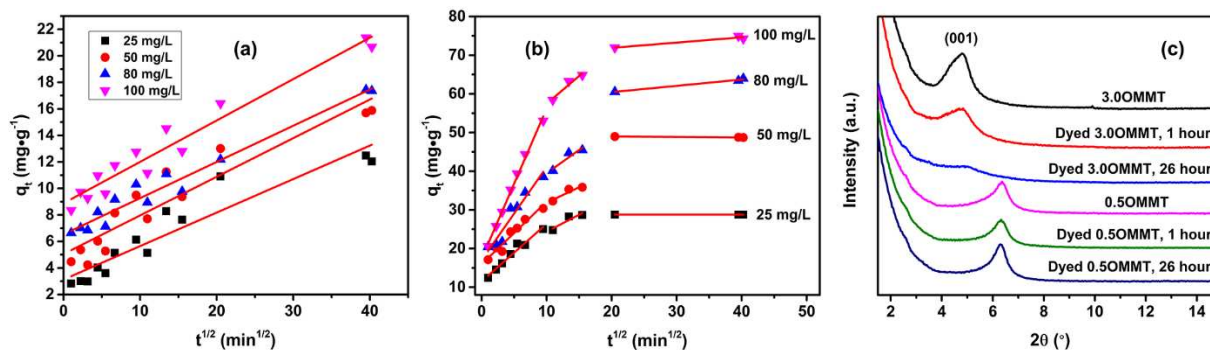
Figure 7. (a) Intra-particle diffusion model fitting for the adsorption of hydrolyzed Remazol Black B from aqueous solutions, onto the 0.5OMMT, with the stated initial hydrolyzed dye loadings, (b) Intra-particle diffusion model fitting for the adsorption of hydrolyzed Remazol Black B from aqueous solutions, onto the 3.0OMMT, with the stated initial hydrolyzed dye loadings, (c) Low-angle XRD patterns of OMMTs and OMMTs dyed for 1 hour or 26 hours.

In order to demonstrate the wider applicability of the results discussed above, two additional widely-used, industrial, anionic dyes with different molecular structures (see ESI) were investigated, as real dyeing wastewaters invariably contain combinations of dyes. The adsorption of hydrolyzed Reactive Blue 19 (anthraquinone dye) and hydrolyzed Reactive Red 195 (single azo dye), each from aqueous solutions, using 3.0OMMT, under the same experimental conditions, were studied. The maximum adsorption capacity for hydrolyzed Reactive Blue 19 was 132 mg/g. This value is 45% greater than the one obtained by Santos *et al*[39] (91 mg/g) who used waste metal hydroxide sludge as the adsorbent. The 3.0OMMT showed a maximum adsorption capacity of 53 mg/g for the hydrolyzed Reactive Red 195, first example of using organo-clays for the adsorption of hydrolyzed Reactive Red 195. After stirring for a commercially-relevant time scale of 1 hour, about 44% of the hydrolyzed Reactive Blue 19 and 16% of the hydrolyzed Reactive Red 195 were removed. It should be noted that in a commercial context the use of 2.0OMMT might be even more economical than the 3.0OMMT as our findings indicate that 2.0OMMT has only slightly smaller

21

dye uptake while utilizing 33% less of the more expensive modifier component. More generally, the above results show that tuning the structure of organo-clays via optimization of modifier loading is a universal and straightforward strategy to enhancement of the adsorption of a broad variety of adsorbates, opening a route towards the treatment of complex dye mixtures that are present in real-life effluents.

Conclusions

Organically modified montmorillonites were prepared via an ion exchange process, at different loadings of CTAB. The modification of the organo-clays was demonstrated by IR, TGA and DSC analyses. TGA, DSC and XRD results indicated that the CTAB molecules were located almost exclusively between the interlayers of the clay at a low modifier loading (0.5 CEC), adopting a monolayer arrangement. When larger amounts of CTAB were used, the CTAB molecules located both in the interlayer spaces of the clay adopting a bilayer arrangement and adsorbed increasingly onto the surface of the clay particles, leading to disordering in the stacking direction of the clay platelets. Saturation for the modification of the organo-clay was observed when 3.0 CEC of CTAB was used during synthesis. The efficiency of dye removal, as tested for the commercially-important hydrolyzed Remazol Black B dye, is directly related to these structural changes. The largest and fastest absolute dye uptake was obtained at the CTAB loading of 3.0 CEC; the dye adsorption efficiency per CTAB molecule was also maximized at this loading. The improved dye uptake relates to improved accessibility of the cationic modifier molecules at this loading due to the expansion of the clay interlamellar spaces, the increased availability of modifier at the clay surface and the disordering along the stacking direction of the clay platelets, confirmed by the adsorption kinetics and XRD results. The resultant organo-clays showed greatly improved adsorption capacity for different dyes, which exhibited potential to be applied commercially, e.g. in the important but

difficult treatment of dye mixtures. The methods used in this work provide a rational how to tune the structure of organo-clays towards enhanced dye adsorption efficiency by utilizing optimized modifier loadings that maximize structural change while avoiding modifier waste. Further improvements in organo-clay adsorbents may be seen when optimizing organo-clay synthesis to enhance the observed effects of interlamellar expansion, surface availability of the cationic modifier and/or disordering along the stacking direction of the clay platelets. Taking these key structural parameters into account, the performance of more unconventional modifiers (e.g. Gemini surfactants, or surfactants with novel functional groups, or surfactants with different chain lengths) may be further improved by applying the principles outlined in this paper.

ASSOCIATED CONTENT

Supporting Information: The supplementary data associated with this article contains determination of the cation exchange capacity of the Na-MMT, Calibration graph for an aqueous solution of hydrolyzed Remazol Black B dye, TGA thermogram and DTGA thermogram of hexadecyltrimethylammonium bromide, dye adsorption kinetics, dimensions of hydrolyzed Remazol Black B molecules, zeta potential of Na-MMT and of OMMT, and molecular structures of the hydrolyzed dyes.

AUTHOR INFORMATION

Corresponding Authors

*Email ID: R.Menzel@leeds.ac.uk   Phone: +44 (0)113 3436407

Email ID: L.Lin@leeds.ac.uk   Phone: +44 (0)113 3436735

Author Contributions

The manuscript was written through contributions of all authors. All authors have given approval to the final version of the manuscript.

Notes

The authors declare no competing financial interest.

REFERENCES

1.   Peng, N.; Hu, D. N.; Zeng, J.; Li, Y.; Liang, L.; Chang, C. Y., Superabsorbent Cellulose-Clay Nanocomposite Hydrogels for Highly Efficient Removal of Dye in Water. *ACS Sustainable Chem. Eng.* **2016,** *4* (12), 7217-7224.

2.   Qin, Y.; Wang, L.; Zhao, C.; Chen, D.; Ma, Y.; Yang, W., Ammonium-Functionalized Hollow Polymer Particles as a pH-Responsive Adsorbent for Selective Removal of Acid Dye. *ACS Appl. Mater. Interfaces.* **2016,** *8* (26), 16690-16698.

3.   Ali, I., New Generation Adsorbents for Water Treatment. *Chem. Rev.* **2012,** *112* (10), 5073-5091.

4.   Liu, X. D.; Yan, L.; Yin, W. Y.; Zhou, L. J.; Tian, G.; Shi, J. X.; Yang, Z. Y.; Xiao, D. B.; Gu, Z. J.; Zhao, Y. L., A Magnetic Graphene Hybrid Functionalized with Beta-Cyclodextrins for Fast and Efficient Removal of Organic Dyes. *J. Mater. Chem. A.* **2014,** *2* (31), 12296-12303.

5.   Kansal, S. K.; Kumari, A., Potential of M. Oleifera for the Treatment of Water and Wastewater. *Chem. Rev.* **2014,** *114* (9), 4993-5010.

6.   Liu, Y.; Luo, C.; Sun, J.; Li, H. Z.; Sun, Z. B.; Yan, S. Q., Enhanced Adsorption Removal of Methyl Orange from Aqueous Solution by Nanostructured Proton-Containing Delta-MnO$_2$. *J. Mater. Chem. A.* **2015,** *3* (10), 5674-5682.

7.   Sengupta, S.; Mondal, R., A Novel Gel-Based Approach to Wastewater Treatment - Unique One-Shot Solution to Potentially Toxic Metal and Dye Removal Problems. *J. Mater. Chem. A.* **2014,** *2* (39), 16373-16377.

8.   Ghosal, A.; Shah, J.; Kotnala, R. K.; Ahmad, S., Facile Green Synthesis of Nickel Nanostructures using Natural Polyol and Morphology Dependent Dye Adsorption Properties. *J. Mater. Chem. A.* **2013,** *1* (41), 12868-12878.

9.   Hadi, P.; Guo, J. X.; Barford, J.; McKay, G., Multilayer Dye Adsorption in Activated Carbons-Facile Approach to Exploit Vacant Sites and Interlayer Charge Interaction. *Environ. Sci. Technol.* **2016,** *50* (10), 5041-5049.

10.   Zhang, L.; Li, X.; Wang, M.; He, Y.; Chai, L.; Huang, J.; Wang, H.; Wu, X.; Lai, Y., Highly Flexible and Porous Nanoparticle-Loaded Films for Dye Removal by Graphene Oxide–Fungus Interaction. *ACS Appl. Mater. Interfaces.* **2016,** *8* (50), 34638-34647.

11.   Alaton, I. A.; Balcioglu, I. A.; Bahnemann, D. W., Advanced Oxidation of a Reactive Dyebath Effluent: Comparison of O$_3$, H$_2$O$_2$/UV-C and TiO$_2$/UV-A Processes. *Water Res.* **2002,** *36* (5), 1143-1154.

12. Chethana, M.; Sorokhaibam, L. G.; Bhandari, V. M.; Raja, S.; Ranade, V. V., Green Approach to Dye Wastewater Treatment using Biocoagulants. *ACS Sustainable Chem. Eng.* **2016,** *4* (5), 2495-2507.

13. Joseph, J. M.; Destaillats, H.; Hung, H.-M.; Hoffmann, M. R., The Sonochemical Degradation of Azobenzene and Related Azo Dyes: Rate Enhancements via Fenton's Reactions. *J. Phys. Chem. A.* **2000,** *104* (2), 301-307.

14. Soler, L.; Magdanz, V.; Fomin, V. M.; Sanchez, S.; Schmidt, O. G., Self-Propelled Micromotors for Cleaning Polluted Water. *ACS Nano.* **2013,** *7* (11), 9611-9620.

15. Chen, F.; Gong, A. S.; Zhu, M.; Chen, G.; Lacey, S. D.; Jiang, F.; Li, Y.; Wang, Y.; Dai, J.; Yao, Y.; Song, J.; Liu, B.; Fu, K.; Das, S.; Hu, L., Mesoporous, Three-Dimensional Wood Membrane Decorated with Nanoparticles for Highly Efficient Water Treatment. *ACS Nano.* **2017,** *11* (4), 4275-4282.

16. Ebrahimi, D.; Pellenq, R. J. M.; Whittle, A. J., Nanoscale Elastic Properties of Montmorillonite Upon Water Adsorption. *Langmuir.* **2012,** *28* (49), 16855-16863.

17. Özcan, A. S.; Özcan, A., Adsorption of Acid Dyes from Aqueous Solutions onto Acid-Activated Bentonite. *J. Colloid Interface Sci.* **2004,** *276* (1), 39-46.

18. Wang, L.; Wang, A., Adsorption Properties of Congo Red from Aqueous Solution onto Surfactant-Modified Montmorillonite. *J. Hazard. Mater.* **2008,** *160* (1), 173-180.

19. Açışlı, Ö.; Karaca, S.; Gürses, A., Investigation of the Alkyl Chain Lengths of Surfactants on their Adsorption by Montmorillonite (Mt) from Aqueous Solutions. *Appl. Clay Sci.* **2017,** *142*, 90-99.

20.   Yang, S.; Gao, M.; Luo, Z., Adsorption of 2-Naphthol on the Organo-Montmorillonites Modified by Gemini Surfactants with Different Spacers. *Chem. Eng. J.* **2014,** *256*, 39-50.

21.   Liu, Y.; Gao, M.; Gu, Z.; Luo, Z.; Ye, Y.; Lu, L., Comparison between the Removal of Phenol and Catechol by Modified Montmorillonite with Two Novel Hydroxyl-Containing Gemini Surfactants. *J. Hazard. Mater.* **2014,** *267*, 71-80.

22.   Luo, Z.; Gao, M.; Ye, Y.; Yang, S., Modification of Reduced-Charge Montmorillonites by a Series of Gemini Surfactants: Characterization and Application in Methyl Orange Removal. *Appl. Surf. Sci.* **2015,** *324*, 807-816.

23.   Dentel, S. K.; Bottero, J. Y.; Khatib, K.; Demougeot, H.; Duguet, J. P.; Anselme, C., Sorption of Tannic Acid, Phenol, and 2,4,5-Trichlorophenol on Organoclays. *Water Res.* **1995,** *29* (5), 1273-1280.

24.   Goswami, S. K.; Ghosh, S.; Mathias, L. J., Thermally Stable Organically Modified Layered Silicates Based on Alkyl Imidazolium Salts. *J. Colloid Interface Sci.* **2012,** *368* (1), 366-371.

25.   Nayar, S. B.; Freeman, H. S., Hydrolyzed Reactive Dyes. Part 1: Analyses via Fast Atom Bombardment and Electrospray Mass Spectrometry. *Dyes Pigm.* **2008,** *79* (2), 89-100.

26.   Xue, G.; Gao, M.; Gu, Z.; Luo, Z.; Hu, Z., The Removal of p-Nitrophenol from Aqueous Solutions by Adsorption using Gemini Surfactants Modified Montmorillonites. *Chem. Eng. J.* **2013,** *218*, 223-231.

27.   Utracki, L. A. Clay-Containing Polymeric Nanocomposites; iSmithers Rapra Publishing: Shropshire, 2004.

28.   Darder, M.; Colilla, M.; Ruiz-Hitzky, E., Biopolymer−Clay Nanocomposites Based on Chitosan Intercalated in Montmorillonite. *Chem. Mater.* **2003,** *15* (20), 3774-3780.

29.   Bromberg, L.; Straut, C. M.; Centrone, A.; Wilusz, E.; Hatton, T. A., Montmorillonite Functionalized with Pralidoxime as a Material for Chemical Protection against Organophosphorous Compounds. *ACS Appl. Mater. Interfaces.* **2011,** *3* (5), 1479-1484.

30.   Vaia, R. A.; Teukolsky, R. K.; Giannelis, E. P., Interlayer Structure and Molecular Environment of Alkylammonium Layered Silicates. *Chem. Mater.* **1994,** *6* (7), 1017-1022.

31.   Ha, B.; Char, K., Conformational Behavior of Dodecyldiamine Inside the Confined Space of Montmorillonites. *Langmuir.* **2005,** *21* (18), 8471-8477.

32.   Xie, W.; Gao, Z. M.; Pan, W. P.; Hunter, D.; Singh, A.; Vaia, R., Thermal Degradation Chemistry of Alkyl Quaternary Ammonium Montmorillonite. *Chem. Mater.* **2001,** *13* (9), 2979-2990.

33.   Zhu, J.; Morgan, A. B.; Lamelas, F. J.; Wilkie, C. A., Fire Properties of Polystyrene-Clay Nanocomposites. *Chem. Mater.* **2001,** *13* (10), 3774-3780.

34.   Zhao, L. Z.; Zhou, C. H.; Wang, J.; Tong, D. S.; Yu, W. H.; Wang, H., Recent Advances in Clay Mineral-Containing Nanocomposite Hydrogels. *Soft Matter.* **2015,** *11* (48), 9229-9246.

35.   He, H.; Frost, R. L.; Bostrom, T.; Yuan, P.; Duong, L.; Yang, D.; Xi, Y.; Kloprogge, J. T., Changes in the Morphology of Organoclays with HDTMA[+] Surfactant Loading. *Appl. Clay Sci.* **2006,** *31* (3–4), 262-271.

36.   Shen, D.; Fan, J.; Zhou, W.; Gao, B.; Yue, Q.; Kang, Q., Adsorption Kinetics and Isotherm of Anionic Dyes onto Organo-Bentonite from Single and Multisolute Systems. *J. Hazard. Mater.* **2009,** *172* (1), 99-107.

37.   Gulnaz, O.; Kaya, A.; Dincer, S., The Reuse of Dried Activated Sludge for Adsorption of Reactive Dye. *J. Hazard. Mater.* **2006,** *134* (1–3), 190-196.

38.   Pochert, A.; Schneider, D.; Haase, J.; Linden, M.; Valiullin, R., Diffusion and Molecular Exchange in Hollow Core Shell Silica Nanoparticles. *Langmuir.* **2015,** *31* (37), 10285-10295.

39.   Santos, S. C. R.; Vilar, V. J. P.; Boaventura, R. A. R., Waste Metal Hydroxide Sludge as Adsorbent for a Reactive Dye. *J. Hazard. Mater.* **2008,** *153* (3), 999-1008.

Table of Contents (TOC) Graphic